

Topological rainbow trapping and broadband piezoelectric energy harvesting of acoustic waves in gradient phononic crystals with coupled interfaces

Xiao-Lei Tang^{a,c}, Tian-Xue Ma^{b,*}, Miso Kim^{c,d}, Yue-Sheng Wang^{a,b,*}

^a*Department of Mechanics, School of Mechanical Engineering, Tianjin University, Tianjin 300350, PR China*

^b*Department of Mechanics, School of Physical Science and Engineering, Beijing Jiaotong University, Beijing 100044, PR China*

^c*School of Advanced Materials Science and Engineering, Sungkyunkwan University (SKKU), Suwon 16419, Republic of Korea*

^d*SKKU Institute of Energy Science and Technology (SIEST), Sungkyunkwan University (SKKU), Suwon 16419, Republic of Korea*

Abstract

Topological phononic crystals (PCs) offer a novel approach to control the behavior of acoustic or elastic waves. In this paper, we design the gradient PC structures with coupled interfaces to realize topological rainbow trapping and broadband acoustic energy harvesting. Based on the geometric symmetry of PC unit cells, we construct the coupled topological interfaces by amalgamating two PCs with distinct topological phases. Also, the gradient modulation of structural parameters along the coupled interfaces is employed for the generation of rainbow trapping. Subsequently, a polyvinylidene fluoride (PVDF) film is mounted along the coupled interfaces of the gradient PC structures, facilitating the conversion of acoustic energy into electrical energy. The numerical and experimental results show that the acoustic waves at different frequencies stop and are amplified at different positions of the coupled interfaces. Compared with the harvester in a bare structure, the topological PC energy harvester significantly enhances the output power at different excited frequencies. In the experiments, the maximum amplification

*Corresponding authors

Email addresses: matx@bjtu.edu.cn (Tian-Xue Ma), yswang@tju.edu.cn (Yue-Sheng Wang)

ratio of the output power reaches 91. Besides, it is demonstrated that the topological rainbow trapping of acoustic waves exhibits robustness against random structural disorders. Notably, the coupled interfaces have broadband and multi-mode features, which are promising for other applications such as selective filtering and sensing enhancement.

Keywords: phononic crystal, topological state, acoustic wave, piezoelectric energy harvesting, rainbow trapping

1. Introduction

Acoustic energy harvesting is emerging as a popular approach for powering small electronic devices. Various transduction mechanisms, such as piezoelectric [1–5], electromagnetic [6–8] and triboelectric [9–12] approaches, have been used to convert acoustic energy into electrical energy. Though sounds are pervasive in daily life their energy is typically characterized by low power density, which limits the efficiency of acoustic energy harvesting. To address the aforementioned issue, sounds need to be concentrated and localized at specified positions. Previous studies have reported several acoustic energy harvesters employing Helmholtz resonators [13] and 1/4-wavelength resonators [14, 15]. Liu *et al.* [16] achieved the acoustic energy harvesting by coupling a piezoelectric patch into the Helmholtz resonator. Yuan *et al.* [17] proposed an acoustic triboelectric nanogenerator based on a 1/4-wavelength resonator system. The proposed system was capable of generating a power output of 4.33 mW under the 100 dB sound pressure level excitation.

Recently, with the studies of phononic crystals (PCs) in diverse disciplines, interest and attempts have also been devoted to their possibility for wave energy harvesting. PCs are artificially designed materials with peculiar wave properties, including negative refraction [18], negative modulus [19] and band gap [20]. Owing to their unique abilities to control acoustic or elastic waves, PCs have been extensively studied by the scientific community for sound transmission [21], cloaking [22] and energy harvesting [23–26]. When a point defect is introduced into a perfect PC, the point defect state of the PC induces an acoustic localization effect. That is, the acoustic waves are concentrated in and around the point defect, and hence, the pressure amplitude is remarkably improved. The acoustic localization effect in PC structures can be harnessed for energy harvesting applications [27–29]. Ma *et al.* [30] combined the PC and the Helmholtz resonator to improve the

sound energy density via wave localization and amplification. In addition, PC lenses [31, 32] are a distinct type of gradient PC structures for the control of wave propagation, in which the effective refractive index of each unit cell is spatially distributed according to specific profiles. Owing to their wave focusing ability, various PC lenses have been constructed for the piezoelectric energy harvesting of elastic [33, 34] or acoustic waves [35]. Kim *et al.* [36] integrated the Helmholtz resonance mechanism with a PC lens to achieve high power output for sounds lower than 1 kHz. Lee *et al.* [37] proposed a gradient PC energy harvester comprising unconventional unit cells derived from machine learning.

The discovery of topological insulators has opened up unprecedented ways for the control of electromagnetic [38], acoustic [39–41] and elastic [42–44] waves. Topologically protected states can be achieved by assembling the materials with different topological phases according to the bulk-edge correspondence. In contrast to conventional wave states, topological interface states (TISs) exhibit excellent robustness against structural defects or imperfections. For instance, despite defects or sharp bands, the TISs can propagate smoothly along the interface under topological protection. In the last decade, acoustic topological insulators have been employed for unidirectional transmission [45, 46], logic operation [47, 48] and acoustic tweezers [49–51]. Besides, the rainbow trapping phenomenon of TISs was reported, in which the TISs at different frequencies are split and stop in different locations [52, 53]. Moreover, the unique wave properties of topological PCs make them a potential candidate for acoustic energy harvesting. Fan *et al.* [54] proposed a one-dimensional (1D) PC tube with TISs to harvest the energy of acoustic waves. Zhao *et al.* [55] theoretically and experimentally demonstrated sub-wavelength acoustic energy harvesting by using the TISs in 1D Helmholtz resonator arrays. Tang *et al.* [56] numerically and experimentally investigated the topological rainbow trapping and energy amplification of acoustic waves in a gradient PC structure. Li *et al.* [57] designed a novel acoustic energy harvesting device based on the TIS of a multi-resonant PC, where the device robustness was improved by the TIS and the operating frequency was lowered by the use of multi-resonant cavities.

However, the piezoelectric energy harvesting of acoustic waves with broadband features and excellent robustness is rarely reported. Notably, in the regime of electromagnetic waves, Elshahat *et al.* [58] observed the rainbow trapping of TISs in the coupled topological interfaces of gradient photonic crystal structures. Interestingly, it was found that the coupling of TISs has

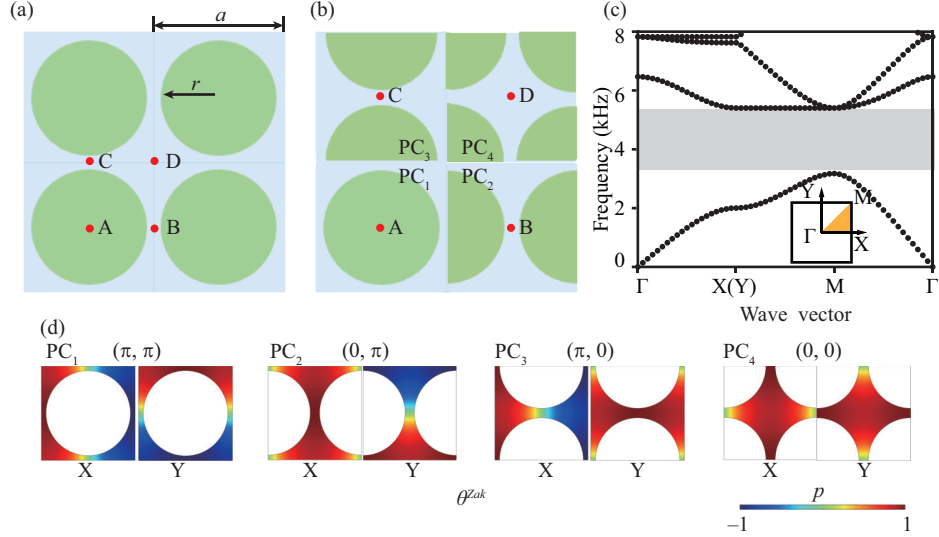


Figure 1: (a) Schematic diagram of the 2D square-latticed PC, in which the polymeric scatterers (green areas) are placed periodically in the air background (light cyan area). (b) Four choices of the PC unit cells, where different inversion centers are marked by red points. (c) Dispersion relations of the PC unit cells, where the band gap is highlighted by gray color. (d) Pressure distributions of the first bulk band at the high symmetry points (X and Y) and the corresponding Zak phases $(\theta_x^{Zak}, \theta_y^{Zak})$.

broadband and multi-mode features. Here, inspired by the above-mentioned study, we propose a gradient PC structure with coupled interfaces to realize broadband topological rainbow trapping and piezoelectric energy harvesting of acoustic waves. The paper is organized as follows. In Section 2, the dispersion relations and topological properties of 2D PCs, as well as the group velocities of TISs, are investigated. Section 3 presents the numerical and experimental results of topological rainbow trapping and sound pressure amplification in designed PC structures with coupled interfaces. Section 4 reports the experimental validation of acoustic energy harvesting. Finally, the conclusions of this paper are provided in Section 5.

2. Band diagram analysis

We construct a 2D square-latticed PC by embedding polymeric scatterers (green areas) in an air background (light cyan area), as sketched in Fig. 1(a). The lattice constant a and the radius of circular scatterers r can describe the geometric configuration of the 2D PC. Thanks to the significant contrast in

acoustic impedance between polymer and air, the polymeric scatterers are considered as acoustically rigid bodies. The mass density and the sound speed of air are $\rho = 1.21 \text{ kg/m}^3$ and $c = 343 \text{ m/s}$, respectively. Throughout this paper, we utilize the finite element method with COMSOL Multiphysics for numerical simulations. Noticeably, this 2D PC has four inversion centers, which are marked as A, B, C and D, respectively [see Fig. 1(a)]. According to the crystal periodicity, four types of PC unit cells can be obtained, as illustrated in Fig. 1(b). The band diagram of the 2D PC is shown in Fig. 1(c), where the lattice constant is $a = 45 \text{ mm}$ and the scatterer radius is $r = 0.45a$. It can be seen from Figs. 1(b) and 1(c) that despite four different choices of unit cells, the band diagrams for the PC are identical.

In this work, the 2D PC is protected by the inversion symmetry, restricting the Zak phase to two values: 0 or π . By studying the symmetry properties of pressure field (p) distribution at the high symmetry points (X and Y) in the Brillouin zone [see Fig. 1(d)], the corresponding $(\theta_x^{Zak}, \theta_y^{Zak})$ of four unit cells can be obtained [59]. Considering the mirror-symmetry of the pressure profile at point Γ , if the pressure profile at the high symmetry points (i.e., X and Y) is symmetric/antisymmetric (S/A), the Zak phase θ_j^{Zak} of the first band is 0 (trivial phase)/ π (non-trivial phase) in the corresponding direction. As depicted in Fig. 1(d), the pressure fields (p) at X(Y) of the four unit cells are A/A, S/A, A/S and S/S, respectively, and hence the corresponding 2D Zak phases $(\theta_x^{Zak}, \theta_y^{Zak})$ are (π, π) , $(0, \pi)$, $(\pi, 0)$ and $(0, 0)$, respectively. In addition, the Zak phase of the first band of the 2D PC along the j ($j = x, y$) direction is defined as $\theta_j^{Zak} = \int dk_x dk_y \text{Tr}[A_j(k_x, k_y)]$, where $A_j(k_x, k_y) = \langle \psi | i\partial k_j | \psi \rangle$ is the Berry connection, ψ denotes the periodic part of the Bloch pressure eigenfunction, and the integration is performed over the first Brillouin zone [60–62]. The numerically calculated Berry connections of different 2D PC unit cells are provided in the Supplementary Material. When two PCs with different topological phases (i.e., Zak phases) are placed adjacently, the combined PC structure will generate topologically protected states at the interface (i.e., TISs). For an acoustic TIS, the acoustic waves propagate steadily along the interface of the PC structure without backscattering.

Next, we combine two kinds of PC unit cells with distinct topological phases ($\theta_x^{Zak} = 0, \theta_y^{Zak} = \pi$) to form a super-cell, as illustrated in Fig. 2(a). One unit cell of PC₂ is sandwiched between ten unit cells of PC₃, forming two coupled topological interfaces. The radius of scatterers along the coupled interfaces (i.e., scatterers in PC₂) is denoted as r_1 . Compared with the

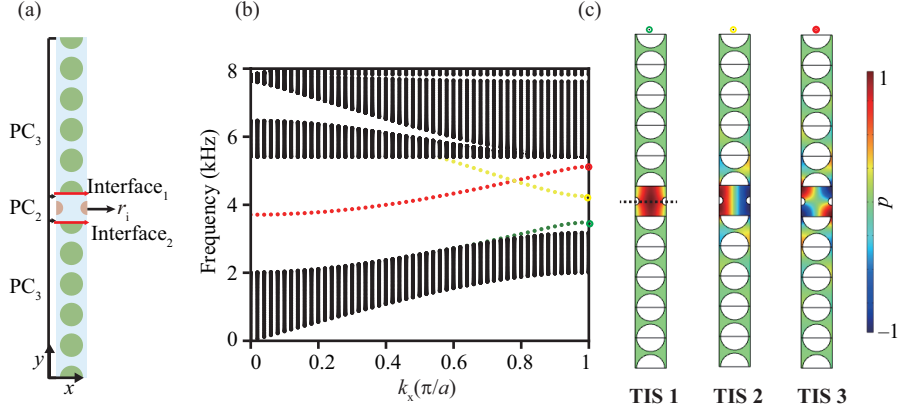


Figure 2: (a) Schematic diagram of the PC super-cell with two coupled interfaces, in which one unit cell of PC₂ is sandwiched between ten unit cells of PC₃. (b) Band diagram of the PC super-cell, where three different TISs (marked by green, yellow and red dots, respectively) emerge inside the band gap. The black dots denote the bulk modes. (c) Pressure distributions of the three TISs at the Brillouin zone boundary $k_x = \pi/a$.

conventional topological interface, the coupled topological interfaces have the superiority of multi-mode and broadband, which are beneficial to multi-mode rainbow trapping and broadband energy harvesting. The TISs in the conventional topological interfaces are discussed in the Supplementary Material. Moreover, the coupled interface region provides sufficient space to host the piezoelectric structures or materials for energy transduction. The band diagram of the PC super-cell is shown in Fig. 2(b), where the black dots denote the bulk states, and the red, yellow and green dots denote the TISs within the band gap. The pressure distributions of the three TISs at $k_x = \pi/a$ are plotted in Fig. 2(c). TISs 1, 2 and 3 exhibit S, S and A patterns with respect to the mirror plane (marked by black dashed line). To facilitate the experiment, TISs 1 and 2 are considered for the realization of rainbow trapping.

It should be noted that in Figs. 3(a) and 3(b), the zero group velocity of TISs 1 and 2 appears at the Brillouin zone boundary $k_x = \pi/a$. The radius of scatterers along the coupled interfaces r_i are changed from $0.04a \sim 0.182a$, and $0.1a \sim 0.28a$ for TISs 1 and 2, respectively. With the increase of r_i , the dispersion curve of TIS 1 (TIS 2) shifts to the lower (higher) frequency region. According to the definition of group velocity v_g ($v_g = \partial\omega/\partial k$ with ω and k being the angular frequency and wave number, respectively), it can be

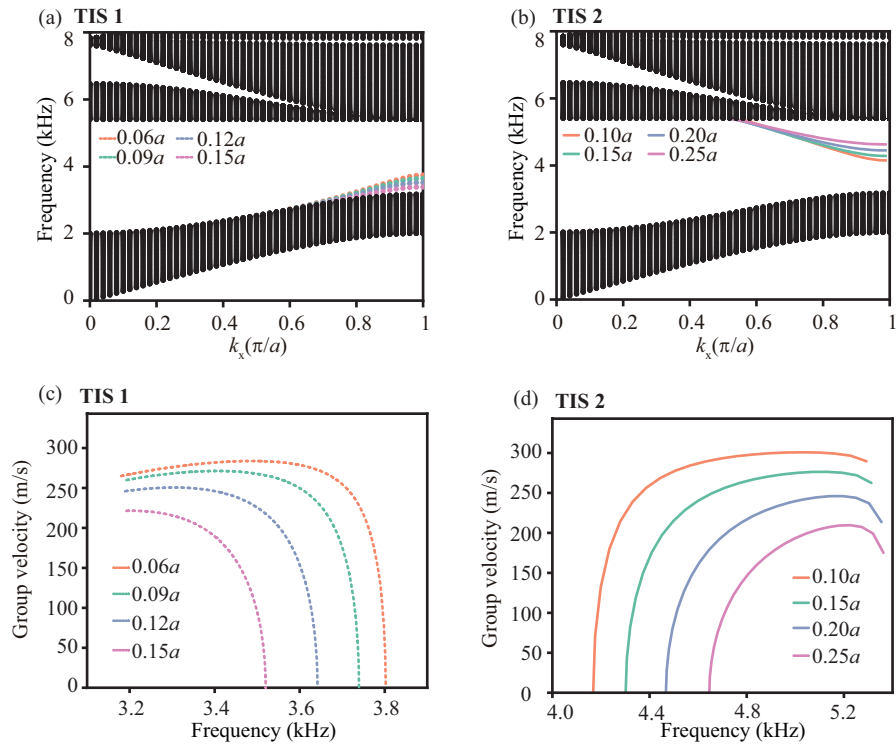


Figure 3: Dispersion curves of TISs 1 (a) and 2 (b) for different radii of scatterers along the coupled interfaces. Group velocity curves of TISs 1 (c) and 2(d) for different radii of scatterers along the coupled interfaces.

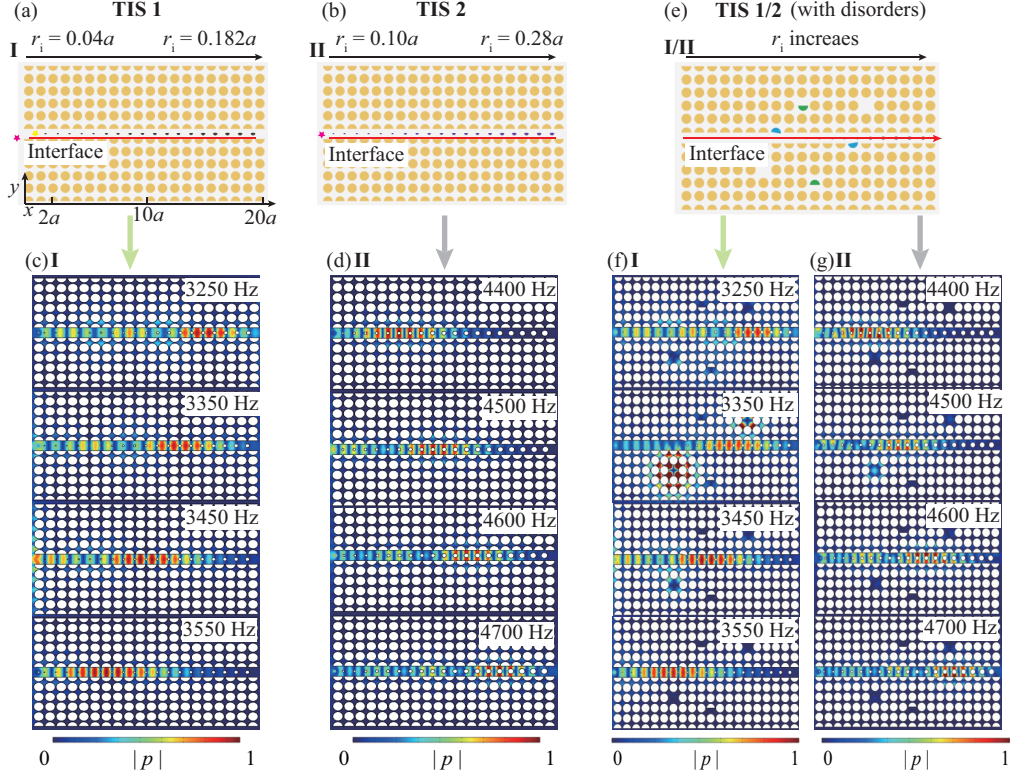


Figure 4: Schematic diagrams of PC samples I (a) and II (b). Topological rainbow trapping in PC samples I (c) and II (d) at different frequencies. (e) Schematic diagram of the PC samples with structural disorders. Topological rainbow trapping in perturbed PC samples I (f) and II (g) at different frequencies.

inferred that the group velocity of the TISs is affected by the geometry of the scatterers along the interfaces. The group velocity v_g of TISs 1 and 2 as a function of r_i is shown in in Figs. 3(c) and 3(d), respectively. As r_i increases, the cut-off frequencies (i.e., $v_g \rightarrow 0$) of TISs 1 and 2 shift to lower and higher frequencies, respectively. As a result, once the acoustic waves enter into the PCs with zero group velocity, they cannot propagate any more and hence be trapped.

3. Topological rainbow trapping

In this section, two configurations of gradient PC structures (with the size of 20×11 unit cells) are constructed to observe topological rainbow trapping,

where PC structures I and II correspond to TISs 1 and 2, respectively, as schematically shown in Figs. 4(a) and 4(b). The radius of scatterers along the coupled interfaces r_i increases linearly along the $+x$ direction. The expression of r_i is described as $r_i = r_0 + (n - 1)\delta_r$, where δ_r is the step variation in r_i and n ($n = 1, 2, \dots, 19$) denotes the position along the interfaces. The configuration of PC structure I (II) is given as follows: $r_0 = 0.04a$ and $\delta_r = 0.00789a$ ($r_0 = 0.1a$ and $\delta_r = 0.01a$). It is known from Section 2 that if the radius of scatterers along the coupled interfaces r_i decreases monotonously, the position of zero group velocity of TISs at different frequencies varies correspondingly. As a result, the gradient PC structures with coupled interfaces generate an intriguing phenomenon, i.e., topological rainbow trapping. In the numerical simulations, a point monopole source (marked by a star) is used to generate acoustic waves and placed on the left side of the PCs. In addition, the perfectly matched layers (PMLs) are utilized to reduce the acoustic wave reflection at the outer boundaries. Furthermore, in order to prove the robustness of topological rainbow trapping, the structural disorders are introduced into the scatterers of PC structures I and II in the following three ways [see Fig. 4(e)]. The rotation angle φ (highlighted by blue color) and the shape (highlighted by green color) are perturbed, as well as the absence of some scatterers is introduced, where φ changes randomly from -10° to 10° .

The frequency responses of the two PC structures with different gradient interfaces are calculated. First, for structure I, the acoustic pressure fields at four selected frequencies of 3250, 3350, 3450 and 3550 Hz are shown in Fig. 4(c). As expected, the position where the acoustic energy is concentrated along the coupled interfaces (marked by the red line) is dependent on the frequency of incident waves. The acoustic waves are well-guided along the coupled interfaces, and the waves at lower frequencies travel further than those at higher frequencies. Interestingly, due to the effect of zero group velocity, the acoustic waves at different frequencies are trapped in different spatial locations. The topological rainbow trapping caused by the gradient interfaces is observed. Then, for structure II, the pressure profiles with the incident waves at 4400, 4500, 4600 and 4700 Hz are presented in Fig. 4(d). Apparently, the topological rainbow trapping is also achieved in PC structure II. In comparison, the results for the perturbed PC structures are plotted in Figs. 4(f) and 4(g). The results for the topological rainbow trapping with and without disorders match well, demonstrating its robustness against structural disorders.

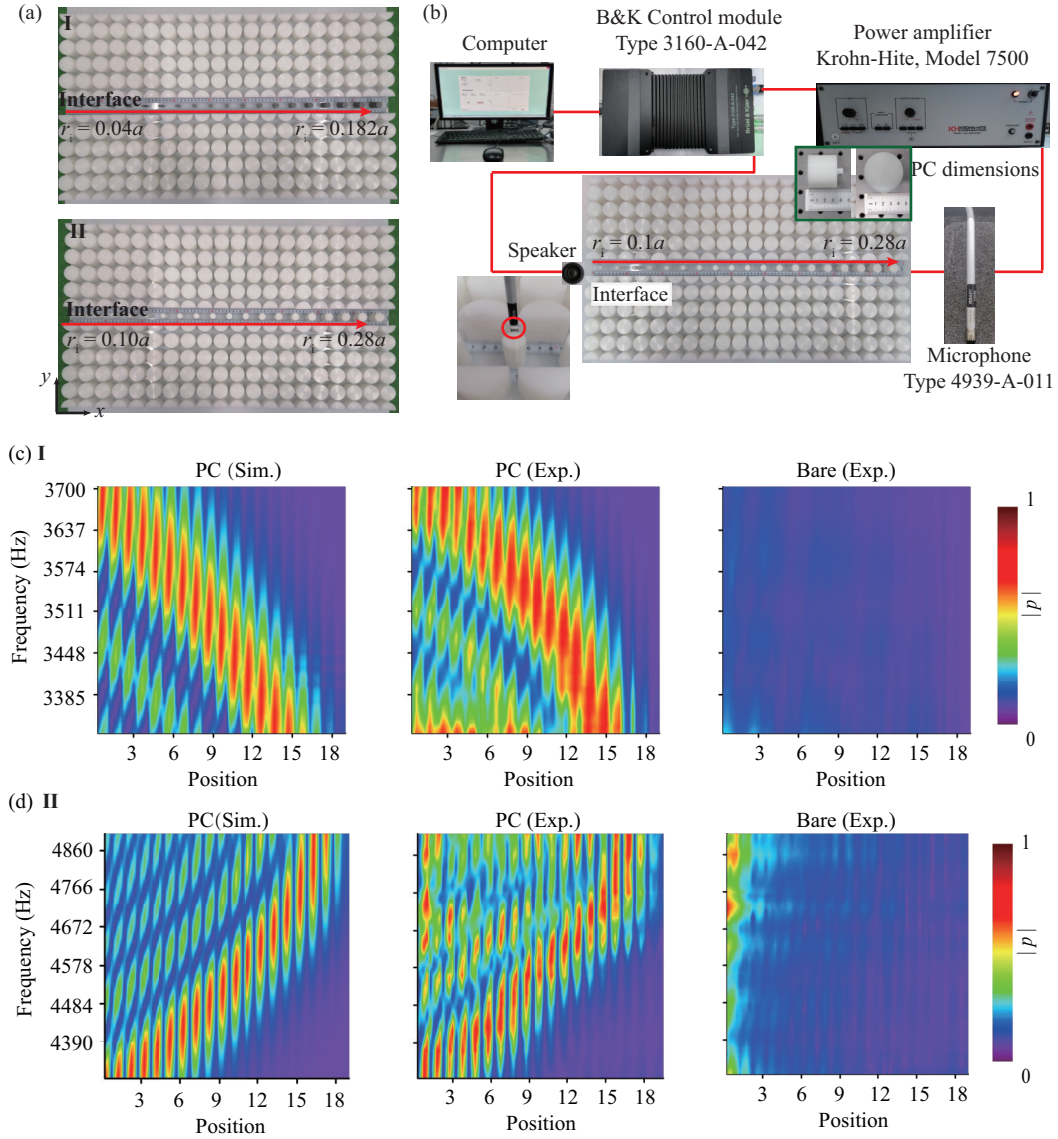


Figure 5: (a) Photographs of the 3D-printed PC samples (I and II). (b) Photograph of the experimental setup, where the inset shows the enlarged view of the drilled holes for inserting the microphone (red wireframe) and the PC dimensions (green wireframe). Numerically calculated and experimentally measured pressure distributions in the perfect PC samples and the bare structure: (c) sample I and (d) sample II.

For the purpose of experimental validation, we fabricate the polymeric PCs via the 3D-printing technique. The photos of the fabricated PC samples are given in Fig. 5(a). The gradient PC samples consist of 20×11 unit cells and the radius of scatterers on the coupled interfaces r_i varies linearly along the $+x$ axis, which are the same as the numerical simulations [see Figs. 4(a) and 4(b)]. The experimental setup is shown in Fig. 5(b). To satisfy the 2D approximation, the PC samples are placed in a planar waveguide with 35 mm height, which are sandwiched by the PMMA and PE plates at the top and bottom, respectively. To accurately measure the acoustic field, we drill 19 holes in the upper PMMA plate of the planar waveguide to accommodate the microphone (Brüel & Kjær, Type 4939-A-011). Thus, the microphone can be inserted into these holes to facilitate the detection of acoustic pressure along the PC interfaces. The signals over the considered frequency range are generated by a generator module (Brüel & Kjær, Type 3160-A-042) and then are amplified by a power amplifier (Krohn-Hite, Model 7500). The amplified signals are played by a loudspeaker, which is placed on the left side of the interfaces of the fabricated PC structures. Additionally, a bare structure (planer waveguide without PCs) is also considered for comparison.

Figures 5(c) and 5(d) show the numerical and experimental results of topological rainbow trapping for PC structures I and II as a function of frequency, respectively. Herein, we will discuss the results of PC structure I in detail. Obviously, the acoustic waves at lower frequencies (e.g., 3385 Hz) can pass through the entire interface of the gradient PC structure. In contrast, the acoustic waves at higher frequencies (e.g., 3700 Hz) can only travel a short distance before being stopped owing to the rainbow trapping effect. The measured and calculated results match well, although the location of the high pressure region in the experiment changes slightly from the numerical prediction. On the other hand, the rainbow trapping of PC structure II is also verified experimentally, as shown in Fig. 5(d). Importantly, compared with the sound pressure in the bare structure, the topological rainbow trapping in the designed PC structures has a significant amplification [see Figs. 5(c) and 5(d)].

Furthermore, to demonstrate the robustness of topological rainbow trapping and acoustic energy amplification, several structural disorders are introduced into PC structures I and II, as shown in Figs. 6(a) and 6(b). The introduced disorders are consistent with the numerical simulations in Fig. 4(c). Figures 6(c) and 6(d) show the calculated and measured pressure distributions in the corresponding frequency ranges for the two disordered PC

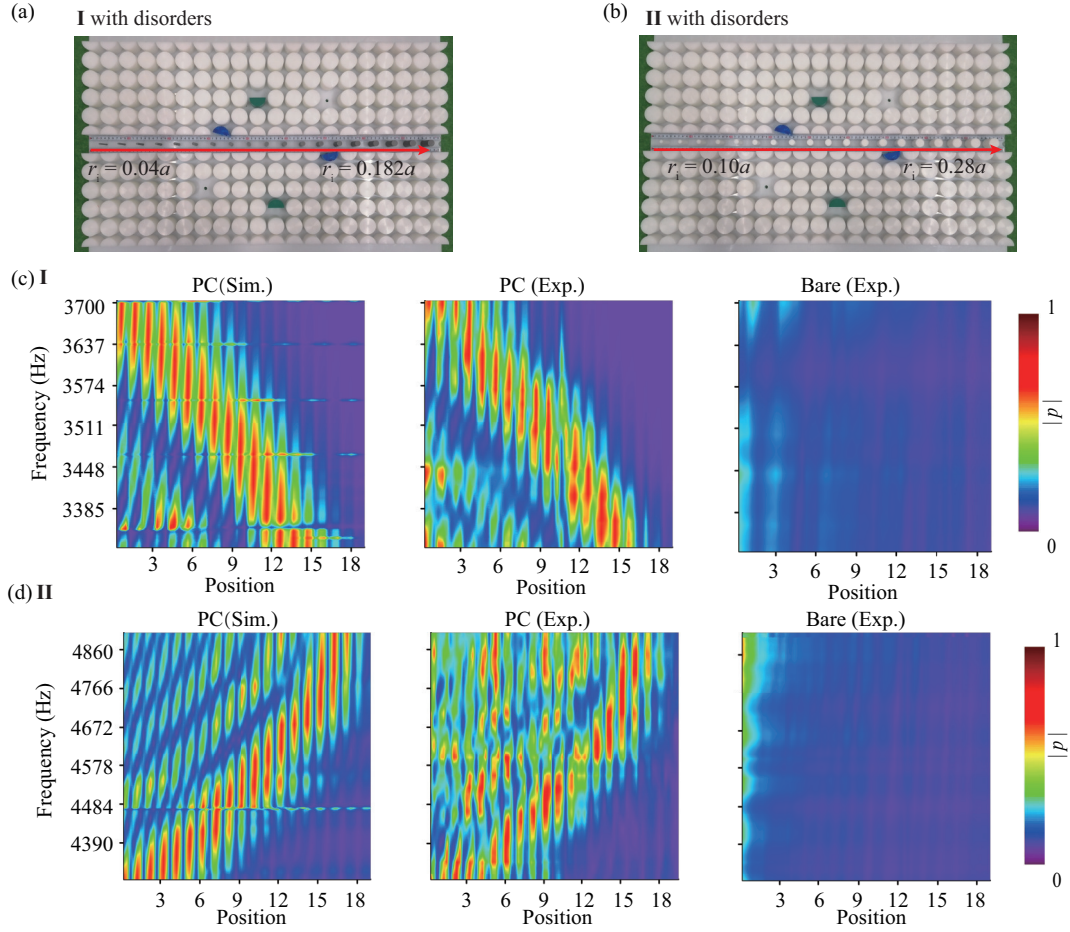


Figure 6: Photographs of PC samples I (a) and II (b) with several structural disorders, where the scatterers are randomly modulated in rotation angle (highlighted by blue color), shape (highlighted by green color) and absence. Numerically calculated and experimentally measured pressure distributions in the disordered PC samples and the bare structure: (c) sample I and (d) sample II.

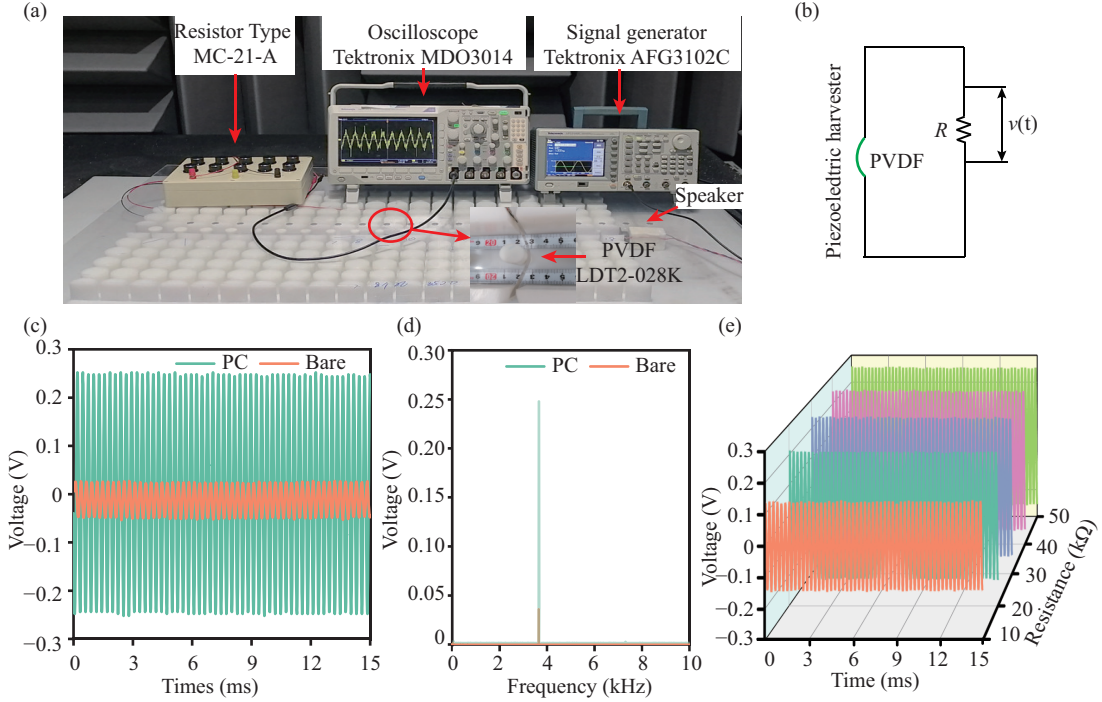


Figure 7: (a) Diagram of the experimental setup for piezoelectric energy harvesting. (b) Schematic of the piezoelectric energy harvesting system. Measured voltage outputs in the time (c) and frequency (d) domains, respectively. (e) Measured voltage outputs in the time domain for different resistance loads.

structures. The numerically calculated and experimentally measured results for topological rainbow trapping are in good agreement. There is a slight deviation at the high pressure position due to experimental errors. Comparing Figs. 5 and 6, we infer that the rainbow trapping of the TISs remains despite the introduction of different types of structural disorders.

4. Experimental validation of acoustic energy harvesting

The experimental setup of the piezoelectric energy harvesting of acoustic waves based on the topological rainbow trapping effect in gradient PCs is plotted in Fig. 7(a). To convert the acoustic energy into the electricity, a PVDF film is placed at the interfaces of the gradient PC structures [see the inset of Fig. 7(a)]. The circuit of the piezoelectric energy harvesting system is schematically illustrated in Fig. 7(b). The acoustic signals are produced

using a signal generator (Tektronix AFG3102C) and then amplified through a power amplifier (Krohn-Hite, Model 7500). The voltage output across the resistance is measured with an oscilloscope (Tektronix, MDO3014). To validate the performance of the PC energy harvester, a continuous sine-wave signal is employed, with the frequencies corresponding to the topological rainbow trapping.

The measured voltage by the piezoelectric film in topological PC structure I at 3675 Hz as a function of time is shown in Fig. 7(c). Moreover, the electric output of the bare structure (without PCs) is measured as the reference. The corresponding voltages in the frequency domain are also plotted in Fig. 7(d). Clearly, the output voltage of the topological PC energy harvester is much higher than that of the reference energy harvester. This is ascribed to the enhancement of acoustic pressure based on topological rainbow trapping. It is noteworthy that the load resistance significantly impacts upon both the voltage and power outputs of the PC piezoelectric energy harvester. Figure 7(e) illustrates the voltage outputs measured from the PC energy harvester under various external load resistances. It is apparent that as the load resistance increases, the voltage amplitude increases as well.

To verify that the proposed PC structures based on the topological rainbow trapping can achieve broadband energy harvesting of acoustic waves, the piezoelectric films are placed at different positions along the structural interfaces, as shown in Fig. 7(a). Because the wave characteristics of the topological rainbow trapping in the spatial and frequency domains, as well as its robustness against to structural disorders have been discussed in Section 3 (see Figs. 5 and 6), we will focus on the performance of piezoelectric energy harvesting. Five frequencies (for PC structure I) from 3450 to 3650 Hz and six frequencies (for PC structure II) from 4450 to 4700 Hz are considered in the energy harvesting experiments. Accordingly, only five positions for Structure I (six positions for Structure II) along the interfaces are employed to host the piezoelectric films. Notably, due to the restriction on the position of piezoelectric films, the excited frequencies are generally not the perfect ones for the energy harvester. The voltage outputs generated by the PC and reference energy harvesters as a function of the load resistance are plotted in Figs. 8(a) and 8(c). It can be seen that as the resistance increases the measured voltage rises monotonically, but its rate of increase gradually degrades and gets saturated at a high resistance. Importantly, compared to the reference structure, the output voltage of the topological PC structures is increased by a factor of 5 ~ 7 times for structure I (i.e., TIS 1) and that

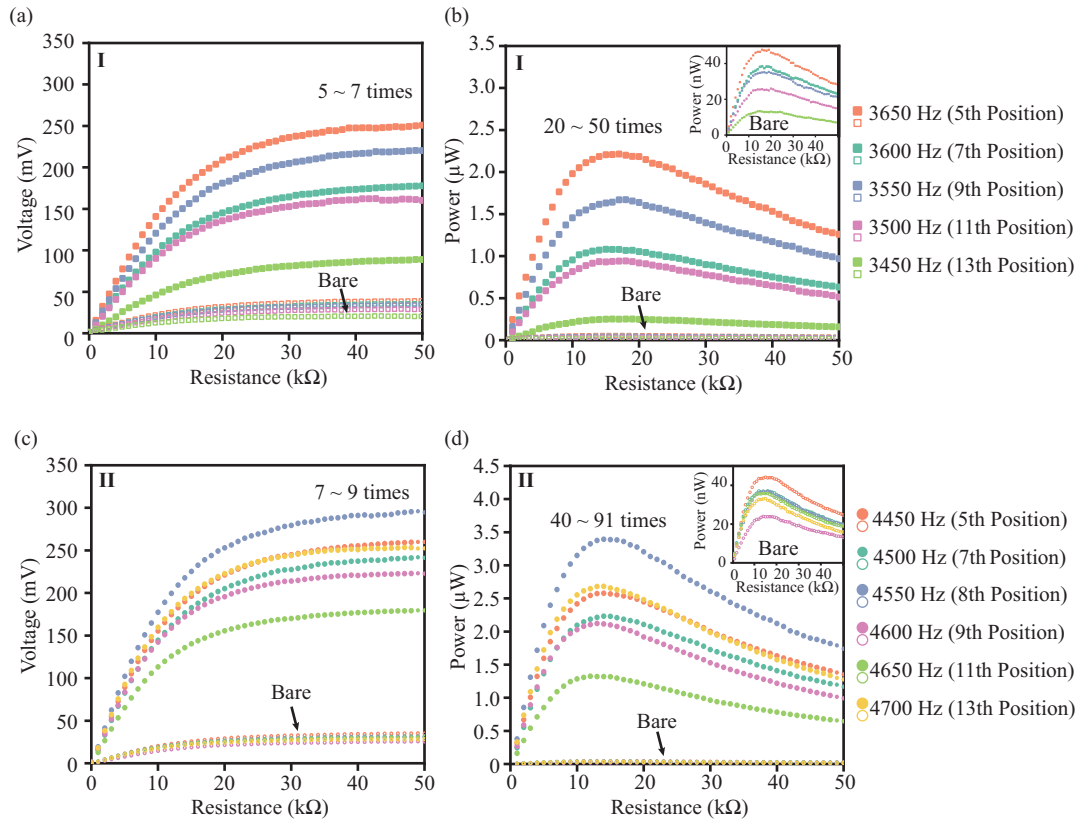


Figure 8: Measured voltage (a, b) and power (c, d) outputs as a function of the resistance load at selected frequencies in PC structures I and II, where the dots and circles denote the outputs obtained from the PC and bare structures, respectively. The results of the bare structure are visually enlarged in the insets of (b) and (d).

of $7 \sim 9$ times for structure II (i.e., TIS 2), achieving the effect of acoustic energy harvesting at all considered frequencies. The power generated by the piezoelectric harvester can be calculated according to Ohm's law $P = U^2/R$, where P , U and R denote the power, voltage and load resistance, respectively. The power output rises with the increase of load resistance until it reaches the maximum values and then starts to decline, as shown in Figs. 8(b) and 8(d). The maximum power generated by the gradient PC structures is about $3.5 \mu\text{W}$ with an external load resistance of $14 \text{ k}\Omega$ at 4550 Hz [see Fig. 8(d)]. Herein, the amplification ratio is defined as the ratio of the power outputs obtained from the PC and reference bare structures. Remarkably, energy harvesting can be achieved from 3300 to 3800 Hz (from 4350 to 4900 Hz) in topological PC structure I (II). The amplification ratios are $20 \sim 50$ and $40 \sim 91$ for the proposed PC harvesters I and II, respectively.

5. Conclusion

In this study, we propose the gradient PC structures with coupled interfaces for topological rainbow trapping and acoustic energy harvesting. The proposed 2D PCs are constructed by polymeric scatterers in the air background, exhibiting a wide band gap with different Zak phases. Thanks to the geometric symmetry, the Zak phase can be tuned by different choices of PC unit cells. The TISs emerge at two coupled interfaces between two PCs with different Zak phases. The results indicate that the acoustic waves of different frequencies separate, stop and are amplified at different positions in the coupled interfaces. In addition, the topological rainbow trapping is robust to randomly structural disorders. To verify the energy harvesting effect, the piezoelectric film is attached at the coupled interfaces of gradient PCs as the piezoelectric energy harvester. The proposed PC structure exhibits the capacity of broadband energy harvesting. Compared with the bare structure, the maximum output power of the topological PC energy harvester is significantly amplified by 91 times. It is noted that the design of coupled interfaces possess the characteristics of multi-mode and broad bandwidth, providing wide application prospects for energy harvesting, sensing and selective filtering.

CRediT authorship contribution statement

Xiao-Lei Tang: Data curation, Formal analysis, Investigation, Methodology, Validation, Visualization, Writing - original draft; Tian-Xue Ma: Con-

ceptualization, Supervision, Formal analysis, Validation, Writing - review & editing; Miso Kim: Funding acquisition, Resources, Writing - review & editing; Yue-Sheng Wang: Funding acquisition, Supervision, Resources, Writing - review & editing.

Declaration of Competing Interest

The authors declare that they have no known competing financial interests or personal relationships that could have appeared to influence the work reported in this paper.

Acknowledgments

We sincerely appreciate Innovative Research Group of NSFC (Grant No. 12021002), National Natural Science Foundation of China (Grant No. 12372087), and the National Research Foundation of Korea grant funded by the Korea government (No.RS-2023-00254689) for the financial support to this study. Xiaolei-Tang is grateful to the support of the China Scholarship Council (Grant No. 202306250172).

DATA AVAILABILITY

The data that support the findings of this study are available from the corresponding author upon reasonable request.

References

- [1] B. Li, J. H. You, Y.-J. Kim, Low frequency acoustic energy harvesting using PZT piezoelectric plates in a straight tube resonator, *Smart Materials and Structures* 22 (2013) 055013.
- [2] J. Choi, I. Jung, C.-Y. Kang, A brief review of sound energy harvesting, *Nano Energy* 56 (2019) 169–183.
- [3] H. Alqaleiby, M. Ayyad, M. R. Hajj, S. A. Ragab, L. Zuo, Effects of piezoelectric energy harvesting from a morphing flapping tail on its performance, *Applied Energy* 353 (2024) 122022.

- [4] P. Eghbali, D. Younesian, S. Farhangdoust, Enhancement of the low-frequency acoustic energy harvesting with auxetic resonators, *Applied Energy* 270 (2020) 115217.
- [5] M. Yuan, Z. Cao, J. Luo, Z. Pang, Low frequency acoustic energy harvester based on a planar Helmholtz resonator, *AIP Advances* 8 (2018).
- [6] F. U. Khan, Izhar, Electromagnetic-based acoustic energy harvester, in: *INMIC*, 2013, pp. 125–130.
- [7] F. U. Khan, M. U. Khattak, Contributed review: Recent developments in acoustic energy harvesting for autonomous wireless sensor nodes applications, *Review of Scientific Instruments* 87 (2016) 021501.
- [8] F. U. Khan, Electromagnetic based acoustic energy harvester for low power wireless autonomous sensor applications, *Sensor Review* 38 (2018) 298–310.
- [9] J. Yang, J. Chen, Y. Liu, W. Yang, Y. Su, Z. L. Wang, Triboelectrification-based organic film nanogenerator for acoustic energy harvesting and self-powered active acoustic sensing, *ACS Nano* 8 (2014) 2649–2657.
- [10] X. Fan, J. Chen, J. Yang, P. Bai, Z. Li, Z. L. Wang, Ultrathin, rollable, paper-based triboelectric nanogenerator for acoustic energy harvesting and self-powered sound recording, *ACS Nano* 9 (2015) 4236–4243.
- [11] Z. Yu, Y. Zhang, Y. Wang, J. Zheng, Y. Fu, D. Chen, G. Wang, J. Cui, S. Yu, L. Zheng, H. Zhou, D. Li, Integrated piezo-tribo hybrid acoustic-driven nanogenerator based on porous MWCNTs/PVDF-TrFE aerogel bulk with embedded pdms tympanum structure for broadband sound energy harvesting, *Nano Energy* 97 (2022) 107205.
- [12] C. Sun, S. Si, J. Liu, Y. Xia, Z. Lin, Q. He, H. Wang, L. Chen, H. Wu, J. Liu, Y. Wu, J. Yang, Flexible, ultra-wideband acoustic device for ultrasound energy harvesting and passive wireless sensing, *Nano Energy* 112 (2023) 108430.
- [13] X. Peng, Y. Wen, P. Li, A. Yang, X. Bai, Enhanced acoustoelectric coupling in acoustic energy harvester using dual Helmholtz resonators,

IEEE Transactions on Ultrasonics, Ferroelectrics, and Frequency Control 60 (2013) 2121–2128.

- [14] B. Li, A. J. Laviage, J. H. You, Y.-J. Kim, Harvesting low-frequency acoustic energy using quarter-wavelength straight-tube acoustic resonator, *Applied Acoustics* 74 (2013) 1271–1278.
- [15] G. Zhu, Y. Zhou, Z. Si, Y. Cheng, F. Wu, H. Wang, Y. Pan, J. Xie, C. Li, A. Chen, R. Wang, J. Sun, A multi-hole resonator enhanced acoustic energy harvester for ultra-high electrical output and machine-learning-assisted intelligent voice sensing, *Nano Energy* 108 (2023) 108237.
- [16] F. Liu, A. Phipps, S. Horowitz, K. Ngo, L. Cattafesta, T. Nishida, M. Sheplak, Acoustic energy harvesting using an electromechanical Helmholtz resonator, *The Journal of the Acoustical Society of America* 123 (2008) 1983–1990.
- [17] M. Yuan, C. Li, H. Liu, Q. Xu, Y. Xie, A 3D-printed acoustic triboelectric nanogenerator for quarter-wavelength acoustic energy harvesting and self-powered edge sensing, *Nano Energy* 85 (2021) 105962.
- [18] R. Zhu, X. Liu, G. Hu, C. Sun, G. Huang, Negative refraction of elastic waves at the deep-subwavelength scale in a single-phase metamaterial, *Nature Communications* 5 (2014) 5510.
- [19] Z. Liu, C. T. Chan, P. Sheng, Analytic model of phononic crystals with local resonances, *Physical Review B* 71 (2005) 014103.
- [20] C. Goffaux, J. Vigneron, Theoretical study of a tunable phononic band gap system, *Physical Review B* 64 (2001) 075118.
- [21] G. Jiang, Y. Liu, Y. Wu, W. Xu, Q. Kong, C. Zhang, Transmission and radiation of acoustic oblique incident through tube arrays based on phononic crystals theory, *Applied Acoustics* 116 (2017) 117–126.
- [22] L.-Y. Zheng, Y. Wu, X. Ni, Z.-G. Chen, M.-H. Lu, Y.-F. Chen, Acoustic cloaking by a near-zero-index phononic crystal, *Applied Physics Letters* 104 (2014) 161904.
- [23] T.-X. Ma, Z.-Y. Li, C. Zhang, Y.-S. Wang, Energy harvesting of Rayleigh surface waves by a phononic crystal Luneburg lens, *International Journal of Mechanical Sciences* 227 (2022) 107435.

- [24] T.-X. Ma, Q.-S. Fan, Z.-Y. Li, C. Zhang, Y.-S. Wang, Flexural wave energy harvesting by multi-mode elastic metamaterial cavities, *Extreme Mechanics Letters* 41 (2020) 101073.
- [25] L. Zhang, T. Tan, Z. Yu, Z. Yan, Topological imbalanced phononic crystal with semi-enclosed defect for high-performance acoustic energy confinement and harvesting, *Nano Energy* 100 (2022) 107472.
- [26] Y. Wang, X. Zhu, T. Zhang, S. Bano, H. Pan, L. Qi, Z. Zhang, Y. Yuan, A renewable low-frequency acoustic energy harvesting noise barrier for high-speed railways using a helmholtz resonator and a pvdf film, *Applied energy* 230 (2018) 52–61.
- [27] L.-Y. Wu, L.-W. Chen, C.-M. Liu, Acoustic energy harvesting using resonant cavity of a sonic crystal, *Applied Physics Letters* 95 (2009) 013506.
- [28] W.-T. Gao, J.-P. Xia, H.-H. Sun, S.-Q. Yuan, Y. Ge, X.-J. Liu, Acoustic energy harvesting for low-frequency airborne sound based on compound Mie resonances, *Applied Physics Express* 12 (2019) 044002.
- [29] A. Yang, P. Li, Y. Wen, C. Yang, D. Wang, F. Zhang, J. Zhang, High-Q cross-plate phononic crystal resonator for enhanced acoustic wave localization and energy harvesting, *Applied Physics Express* 8 (2015) 057101.
- [30] K. Ma, T. Tan, Z. Yan, F. Liu, W.-H. Liao, W. Zhang, Metamaterial and Helmholtz coupled resonator for high-density acoustic energy harvesting, *Nano Energy* 82 (2021) 105693.
- [31] Y. Jin, B. Djafari-Rouhani, D. Torrent, Gradient index phononic crystals and metamaterials, *Nanophotonics* 8 (2019) 685–701.
- [32] G. Lee, S.-J. Lee, J. Rho, M. Kim, Acoustic and mechanical metamaterials for energy harvesting and self-powered sensing applications, *Materials Today Energy* 37 (2023) 101387.
- [33] F. Akbari-Farahani, S. Ebrahimi-Nejad, From defect mode to topological metamaterials: A state-of-the-art review of phononic crystals & acoustic metamaterials for energy harvesting, *Sensors and Actuators A: Physical* (2023) 114871.

- [34] J. Hyun, W. Choi, M. Kim, Gradient-index phononic crystals for highly dense flexural energy harvesting, *Applied Physics Letters* 115 (2019) 173901.
- [35] A. Allam, K. Sabra, A. Erturk, Sound energy harvesting by leveraging a 3D-printed phononic crystal lens, *Applied Physics Letters* 118 (2021) 103504.
- [36] S. Kim, J. Choi, H. M. Seung, I. Jung, K. H. Ryu, H.-C. Song, C.-Y. Kang, M. Kim, Gradient-index phononic crystal and Helmholtz resonator coupled structure for high-performance acoustic energy harvesting, *Nano Energy* 101 (2022) 107544.
- [37] S. Lee, W. Choi, J. W. Park, D.-S. Kim, S. Nahm, W. Jeon, G. X. Gu, M. Kim, S. Ryu, Machine learning-enabled development of high performance gradient-index phononic crystals for energy focusing and harvesting, *Nano Energy* 103 (2022) 107846.
- [38] L. Lu, J. D. Joannopoulos, M. Soljačić, Topological photonics, *Nature Photonics* 8 (2014) 821–829.
- [39] Y.-F. Chen, Z.-G. Chen, H. Ge, C. He, X. Li, M.-H. Lu, X.-C. Sun, S.-Y. Yu, X. Zhang, Various topological phases and their abnormal effects of topological acoustic metamaterials, *Interdisciplinary Materials* 2 (2023) 179–230.
- [40] S. Yin, L. Ye, H. He, M. Ke, Z. Liu, Acoustic valley-locked waveguides in heterostructures of a Square lattice, *Physical Review Applied* 18 (2022) 054073.
- [41] S. Zheng, X. Man, Z.-L. Kong, Z.-K. Lin, G. Duan, N. Chen, D. Yu, J.-H. Jiang, B. Xia, Observation of fractal higher-order topological states in acoustic metamaterials, *Science Bulletin* 67 (2022) 2069–2075.
- [42] T.-X. Ma, J. Liu, C. Zhang, Y.-S. Wang, Topological edge and interface states in phoxonic crystal cavity chains, *Physical Review A* 106 (2022) 043504.
- [43] Z. Ma, Y. Liu, Y.-X. Xie, Y.-S. Wang, A simple elastic phononic crystal plate with adjustable topological valley transmission paths, *Extreme Mechanics Letters* 57 (2022) 101910.

- [44] T.-X. Ma, Q.-S. Fan, C. Zhang, Y.-S. Wang, Flexural wave energy harvesting by the topological interface state of a phononic crystal beam, *Extreme Mechanics Letters* 50 (2022) 101578.
- [45] B.-Z. Xia, T.-T. Liu, G.-L. Huang, H.-Q. Dai, J.-R. Jiao, X.-G. Zang, D.-J. Yu, S.-J. Zheng, J. Liu, Topological phononic insulator with robust pseudospin-dependent transport, *Physical Review B* 96 (2017) 094106.
- [46] C. He, X. Ni, H. Ge, X.-C. Sun, Y.-B. Chen, M.-H. Lu, X.-P. Liu, Y.-F. Chen, Acoustic topological insulator and robust one-way sound transport, *Nature Physics* 12 (2016) 1124–1129.
- [47] Y.-J. Lu, Y. Wang, Y. Ge, S.-Q. Yuan, D. Jia, H.-X. Sun, X.-J. Liu, Multifunctional acoustic logic gates by valley sonic crystals, *Applied Physics Letters* 121 (2022) 123506.
- [48] H. Pirie, S. Sadhuka, J. Wang, R. Andrei, J. E. Hoffman, Topological phononic logic, *Physical Review Letters* 128 (2022) 015501.
- [49] H. Dai, L. Liu, B. Xia, D. Yu, Experimental realization of topological on-chip acoustic tweezers, *Physical Review Applied* 15 (2021) 064032.
- [50] P. Liu, H. Li, Z. Zhou, Y. Pei, Topological acoustic tweezer and pseudo-spin states of acoustic topological insulators, *Applied Physics Letters* 120 (2022) 222202.
- [51] L. Du, G. Hu, Y. Hu, Q. Wang, Acoustic forceps based on focused acoustic vortices with different topological charges, *Sensors* 23 (2023) 6874.
- [52] G. J. Chaplain, J. M. De Ponti, G. Aguzzi, A. Colombi, R. V. Craster, Topological rainbow trapping for elastic energy harvesting in graded Su-Schrieffer-Heeger systems, *Physical Review Applied* 14 (2020) 054035.
- [53] Z. Tian, C. Shen, J. Li, E. Reit, H. Bachman, J. E. Socolar, S. A. Cummer, T. Jun Huang, Dispersion tuning and route reconfiguration of acoustic waves in valley topological phononic crystals, *Nature Communications* 11 (2020) 762.
- [54] L. Fan, Y. He, X.-a. Chen, X. Zhao, Acoustic energy harvesting based on the topological interface mode of 1D phononic crystal tube, *Applied Physics Express* 13 (2019) 017004.

- [55] D. Zhao, X. Chen, P. Li, X.-F. Zhu, Subwavelength acoustic energy harvesting via topological interface states in 1D Helmholtz resonator arrays, *AIP Advances* 11 (2021) 015241.
- [56] X.-L. Tang, T.-X. Ma, Y.-S. Wang, Topological rainbow trapping and acoustic energy amplification in two-dimensional gradient phononic crystals, *Applied Physics Letters* 122 (2023) 112201.
- [57] B. Li, H. Chen, B. Xia, L. Yao, Acoustic energy harvesting based on topological states of multi-resonant phononic crystals, *Applied Energy* 341 (2023) 121142.
- [58] S. Elshahat, M. S. M. Esmail, H. Yuan, S. Feng, C. Lu, Broadband multiple topological rainbows, *Annalen der Physik* 534 (2022) 2200137.
- [59] M. Xiao, G. Ma, Z. Yang, P. Sheng, Z. Zhang, C. T. Chan, Geometric phase and band inversion in periodic acoustic systems, *Nature Physics* 11 (2015) 240–244.
- [60] J. K. Asbóth, L. Oroszlány, A. Pályi, A short course on topological insulators, *Lecture Notes in Physics* 919 (2016) 166.
- [61] F. Zangeneh-Nejad, R. Fleury, Topological Fano resonances, *Physical Review Letters* 122 (2019) 014301.
- [62] C. Lu, C. Wang, M. Xiao, Z. Zhang, C. T. Chan, Topological rainbow concentrator based on synthetic dimension, *Physical Review Letters* 126 (2021) 113902.